Inorganic Chemistry

Article

pubs.acs.org/IC

Electronic Structures and Magnetism of $SrFeO_2$ under Pressure: A First-Principles Study

Mavlanjan Rahman, Yao-zhuang Nie, and Guang-hua Guo*

School of Physics and Electronics, Central South University, Changsha 410083, People's Republic of China

ABSTRACT: We have studied the electronic structures and magnetism of $SrFeO_2$ under pressure by first-principles calculations in the framework of density functional theory (DFT) with GGA+U and HSE06 hybrid functionals, respectively. The pressure-induced spin transition from $S = 2$ to $S = 1$ and the antiferromagnetic−ferromagnetic (AFM-FM) transition observed in experiment are well reproduced by taking the site repulsion U and its pressure dependence into account. The electronic structure and its change with the pressure can be qualitatively understood in an ionic model together with the hybridization effects between the Fe 3d and O 2p states. It is found that the pressure leads to a change in Fe 3d electronic configuration from $(d_{z^2})^2(d_{xz}d_{yz})^2(d_{xy})^1(d_{x^2-y^2})^1$ under ambient conditions to $(d_{z^2})^2(d_{xz}d_{yz})^3(d_{xy})^1(d_{x^2-y^2})^0$ at high pressure. As a result, the spin state transits from $S = 2$ to $S = 1$ and both the antiferromagnetic intralayer Fe−O−Fe superexchange interaction and the interlayer Fe−Fe direction exchange coupling at ambient pressure become ferromagnetic at high pressure according to the Goodenough−Kanamori (G-K) rules. Additionally, our calculations predict another spin transition from $S = 1$ to $S = 0$ at pressures of about 220 GPa.

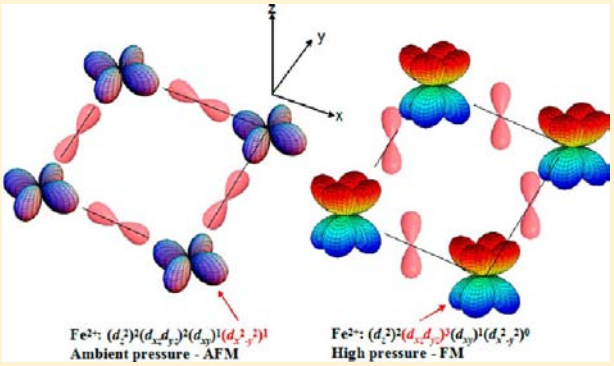

I. INTRODUCTION

Recently, the newly synthesized compound $SrFeO_2$ with a crystal structure similar to that of $SrCuO_2$, the parent compound for a high-T_c superconductor, has attracted much attention because of its interesting properties and potential applications.[1−4] $SrFeO_2$ has an infinite layered structure, being composed of two-dimensional FeO_2 layers with corner-sharing FeO_4 squares separated by Sr^{2+} ions (Figure 1). Typically, Fe d^6 is either tetrahedrally or octahedrally coordinated, rarely in a square-planar environment. Only in the mineral gillespite, $BaFeSi_4O_{10}$, is square-planar coordination of oxygen around iron to be found.[5] After the synthesis of $SrFeO_2$, subsequent studies reported several new compounds with the FeO_4 square-planar motif, such as $(Sr,Ba,Ca)FeO_2$, $Sr_3Fe_2O_5$, and $Sr_3Fe_2O_4Cl_2$.[6] There are some interesting puzzles about $SrFeO_2$. One of them is the Fe^{2+} 3d orbital electron occupation; the last lone down-spin electron occupies the d_{z^2} orbital rather than the degenerate $d_{xz}d_{yz}$ orbital as expected by crystal field theory,[7] which prevents the system from Jahn−Teller distortion. Furthermore, the compound shows three-dimensional antiferromagnetic (AFM) order with a very high Néel temperature (~473 K)[2] in spite of its two-dimensional crystal structure. Recently, it was reported[8] that the $SrFeO_2$ exhibits a spin transition from the high-spin state $S = 2$ to the intermediate-spin state $S = 1$ at a pressure of ~33 GPa, almost simultaneously accompanied by a typical Mott insulator−metal transition and an AFM-FM transition. Usually, the spin transition occurs in compounds of octahedrally coordinated 3d transition metal ions, rarely in compounds of two-dimensional layer structure. In fact, $SrFeO_2$ represents the first spin state transition in a 4-fold coordinated metal ion center.[9−11] So far, there are still problems needing to be solved

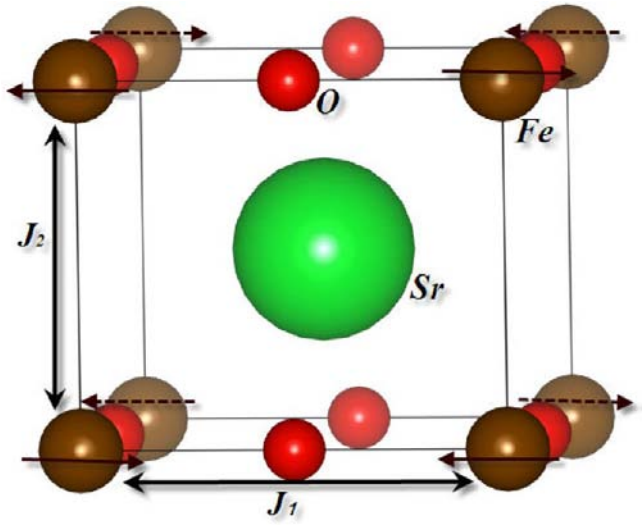

Figure 1. Perspective view of the tetragonal structure of $SrFeO_2$. Green, black, and red balls represent the Sr, Fe, and O atoms, respectively. J_1 and J_2 denote the intralayer Fe−O−Fe superexchange interaction and the interlayer Fe−Fe direct exchange interaction, respectively. Arrows indicate the spin orientations of Fe ions.

Received: June 25, 2013
Published: October 23, 2013

   dx.doi.org/10.1021/ic401615r | Inorg. Chem. 2013, 52, 12529−12534

about $SrFeO_2$. For example, there are different explanations about the absence of the Jahn−Teller distortion.[2,3] Although Kawakami et al.[8] gave a nice explanation of the spin transition under pressure, the mechanisms of the AFM order at ambient pressure and the pressure-induced AFM-FM phase transition as well as the insulator−metal transition are unclear.

In this paper, we report results on the electronic structures and magnetism of $SrFeO_2$ under pressure obtained from our first-principles calculations. Our work is based on the generalized gradient approximation plus on site repulsion U (GGA+U) method and HSE06 hybrid functional. We aim to find out the mechanisms of these ordered phases and their transitions under pressure.

II. COMPUTATION

We performed first-principles calculations using the program PWSCF included in the QUANTUM ESPRESSO package.[12] Because the generalized gradient approximation (GGA)[13] usually fails to predict the ground state of transition-metal oxides,[14] generalized gradient approximation plus on site repulsion (GGA+U)[15] (in combination with ultrasoft pseudopotentials[16]) and HSE06 hybrid functionals[17] (together with norm-conserving pseudopotentials[18]) are used in our calculations. The total energy and the density of state (DOS) for $SrFeO_2$ were calculated at different pressures, from ambient pressure to 240 GPa. The crystal structure of $SrFeO_2$ belongs to the space group $P4/mmm$ with the experimental lattice parameters $a = b = 3.985$ Å and $c = 3.458$ Å (Figure 1). We considered the paramagnetic (PM) state, the FM state, and four kinds of AFM states, namely, AF1 with $\boldsymbol{q}$ = (0.5, 0.5, 0.5), AF2 with $\boldsymbol{q}$ = (0.0, 0.0, 0.5), AF3 with $\boldsymbol{q}$ = (0.5, 0.5, 0.0), and AF4 with $\boldsymbol{q}$ = (0.5, 0.0, 0.5), respectively. For the FM state we worked with the primitive cell depicted in Figure 1. For other AFM states supercells were used. The plane wave energy cutoff was set to 400 eV, and an 8 × 8 × 8 grid was used for Brillouin-zone integration in all of our calculations. These calculation parameters were chosen to guarantee the total energy error in 1 meV per atom. The pressure dependence of U was set according to the linear relation $U = 5 - P/10$, where P is in GPa and U is in eV.

III. RESULTS AND DISCUSSION

We first determined the magnetic stable state at ambient pressure. For GGA+U calculations, we found that the basic conclusions remained unchanged when U varied from 3 to 6 eV under ambient pressure. For $U < 3$ eV, the ground state of $SrFeO_2$ is FM metallic, which is in disagreement with the experimental results. For $U > 6$ eV, the obtained spin moment is obviously larger than experimental data. The results reported here are for the choice of $U = 5$ eV. Our calculations show that the ground state is an AF1Mott insulator with a magnetic moment of 3.7 μ_B for each iron atom, which is in good agreement with the experimental results.[1]

Figure 2 gives the calculated density of states (DOS) for Fe at ambient pressure, which shows that Fe 3d orbitals have a large exchange splitting, larger than the splitting of the crystal field. As a result, Fe^{2+} (d^6) is in the high-spin state ($S = 2$) at ambient pressure. In fact, the electronic structure of $SrFeO_2$ can be qualitatively understood in an ionic model together with the hybridization effects between the Fe 3d and O 2p states. According to crystal field theory, the degeneracy of 3d orbitals is lifted due to the ligands. In aboctahedral crystal field, the lobes of e_g are directed toward negatively charged ligands, while the lobes of t_{2g} are not directed toward them. Therefore the energy of e_g is higher than that of t_{2g}. The square-planar coordination can be imagined as a result when two ligands on the z axis of an octahedron are removed from the complex, leaving only the ligands in the x−y plane. The orbital splitting

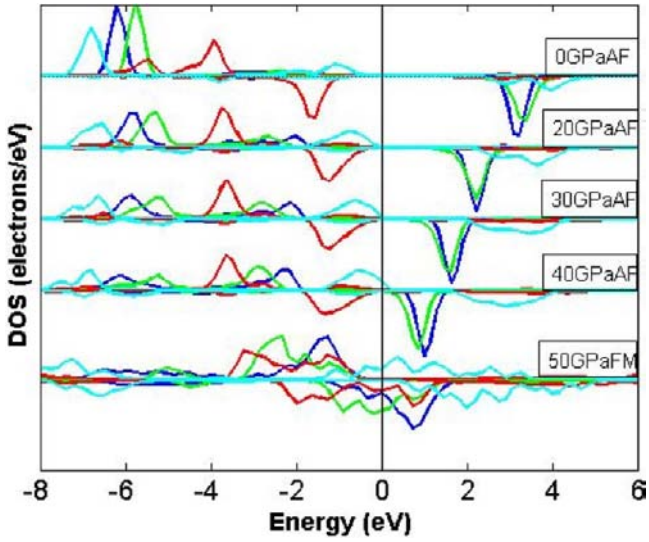

Figure 2. Calculated densities of state for d orbitals of Fe^{2+} at different pressures: (blue line) d_{xy} orbital; (green line) $d_{xz}d_{yz}$ orbital; (red line) d_{z^2} orbital; (cyan line) $d_{x^2-y^2}$ orbital.

diagram for square-planar coordination can thus be derived from the octahedral diagram. As ligands move away along the z axis, d orbitals with a z component will fall in energy level. The d_{z^2} orbital falls the most, as its electrons are concentrated in lobes along the z axis. The d_{xz} and d_{yz} orbitals also drop in energy, but not as much. Conversely, the $d_{x^2-y^2}$ and the d_{xy} orbitals increase in energy level. Therefore, the d orbitals split into four groups: i.e., d_{z^2} (a_{1g}), $d_{xz}d_{yz}$ (e_g), d_{xy} (a_{2g}), and $d_{x^2-y^2}$ (b_{1g}) (in energy sequence from low to high level). The d_{z^2} orbital or the degenerate $d_{xz}d_{yz}$ pair of orbitals will lie lowest in energy and the $d_{x^2-y^2}$ orbital lies highest in energy and the d_{xy} lies next highest. Calculations[19] based on the assumption of the point−dipole model show the order of increasing energy is $d_{xz}d_{yz} < d_{z^2} < d_{xy} < d_{x^2-y^2}$. However, for D_{4h} symmetry, the 4s and d_{z^2} orbitals of a transition-metal ion have the same symmetry, a_{1g}. 4s and d_{z^2} construct molecular orbitals with the a_{1g} orbital of the ligands. This lowers the energy of d_{z^2} further and may change the order of energy levels.[5] In fact, $BaFeSi_4O_{10}$, the only square-planar coordination of oxygen around iron found earlier,[4] shows the 3d orbital of Fe^{2+} with energy order $d_{z^2} < d_{xz}d_{yz} < d_{xy} < d_{x^2-y^2}$. According to molecular orbital theory, the interaction between $d_{x^2-y^2}$ and the four ligands is the strongest. They form σ bonding and antibonding states. Bonding states have the characteristics of ligands, and the energy level order differs from that of crystal field or even the reverse. Antibonding states have characteristic of transition-metal ions and the energy level order with crystal field splitting as shown in Figure 3. It is clear that DOS from our first-principles calculations (Figure 2) are consistent with what is expected by ligand field theory and molecular orbital theory. We find that the antibonding state orbitals on the energy range from −5 to 0 eV and note that the d_{z^2} orbital is the lowest one. The electronic configurations are $(d_{z^2})^1(d_{xz}d_{yz})^2(d_{xy})^1(d_{x^2-y^2})^1$ for the up-spin state and $(d_{z^2})^1(d_{xz}d_{yz})^0(d_{xy})^0(d_{x^2-y^2})^0$ for the down-spin state. Therefore, the last minority-spin electron of Fe^{2+} (d^6) occupies the d_{z^2} orbital rather than the degenerate $d_{xz}d_{yz}$ orbitals, which prevents the system from Jahn−Teller distortion. Tsujimoto et al. assumed the $(d_{z^2})^1(d_{xz}d_{yz})^3(d_{xy})^1(d_{x^2-y^2})^1$ electronic configuration for the 3d electrons of Fe^{2+} according to their experimental data[1] and

dx.doi.org/10.1021/ic401615r | Inorg. Chem. 2013, 52, 12529−12534

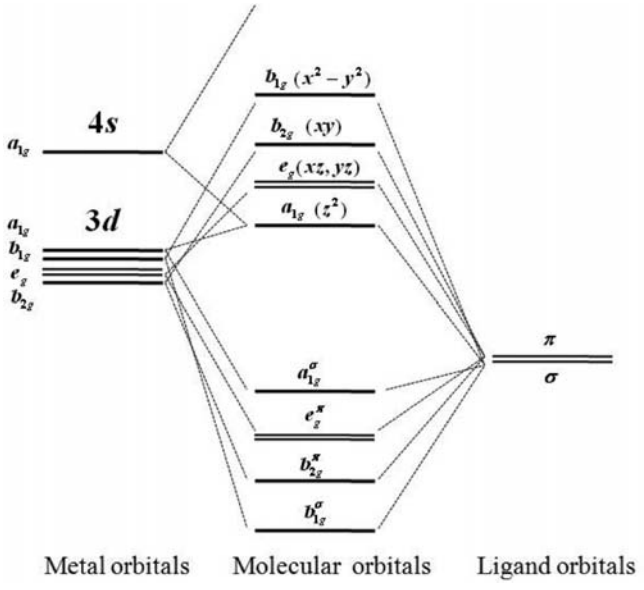

Figure 3. Relative molecular orbital energies for $SrFeO_2$. For clarity, spin splitting is not shown.

attributed it to D_{4h} point group symmetry. Because there are no signs of structural instability from their experiment, they argued that the strong covalent bond between Fe and O inhibits the Jahn−Teller distortion. Xiang et al.[2] and Pruneda et al.[3] carried out first-principles calculations and obtained the same results as ours. However, they made different interpretations of the results. Xiang et al. regarded that the lowest energy orbital being d_{z^2} rather than the degenerate $d_{xz}d_{yz}$, as expected from crystal field theory, comes from the reduction of Coulomb energy along the z direction. Meanwhile, the $(d_{z^2})^2$ occupations are consistent with the experimental result that spin moments are perpendicular to te c axis according to their spin−orbital coupling calculations. Prundera et al. argued that d_{z^2} orbitals are not the lowest-lying ones for both the majority- and minority-spin electrons of Fe^{2+}. They considered that the double occupation of the d_{z^2} orbital of Fe^{2+} may seem counterintuitive on the basis of common knowledge in molecular and solid-state chemistry. They attributed the $(d_{z^2})^2$ occupations to the reduction of spin splitting of d_{z^2} orbitals due to the interaction between d_{z^2} and 4s orbitals of Fe^{2+}.

The G-type AFM state of $SrFeO_2$ at ambient pressure comes from both antiferromagnetic intraplayer and interlayer exchange interactions. According to the Fe 3d $(d_{z^2})^2(d_{xz}d_{yz})^2(d_{xy})^1(d_{x^2-y^2})^1$ electronic configuration, we see that the intraplane superexchange interaction is due to $d_{x^2-y^2}$ orbitals of two adjacent Fe^{2+} ions through O p_σ and d_{xy} orbitals through p_π (Figure 4a). If the single unpaired electrons of two $d_{x^2-y^2}$ orbitals are coupled antiferromagnetically through p_σ, the electrons can be delocalized over the M−O−M unit, thus lowering the kinetic energy. If the electrons on the $d_{x^2-y^2}$ orbitals are coupled ferromagnetically, the delocalized configurations mentioned above are prevented by the Pauli exclusion principle. The ferromagnetic configuration therefore costs more energy. For the same reason, the single unpaired electrons of two d_{xy} orbitals should be coupled antiferromagnetically through p_π. Now let us look at the degenerate $d_{xz}d_{yz}$ orbitals. Along the z axis, adjacent d_{xz} orbitals have weak π bonds, as do d_{yz} orbitals (Figure 4b). If two unpaired electrons of degenerate $d_{xz}d_{yz}$ orbitals are coupled antiferromagnetically to other two

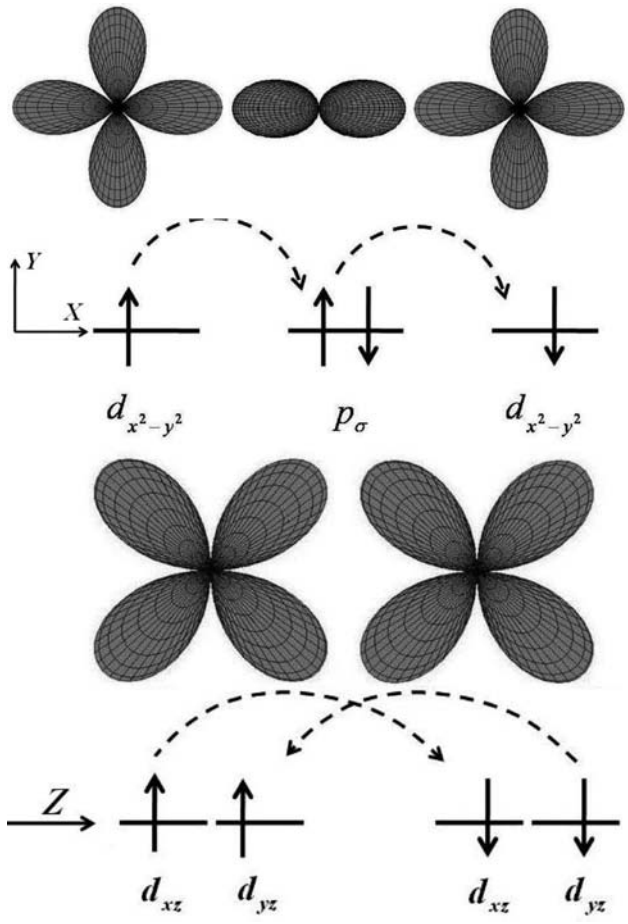

Figure 4. Illustrations of the intralayer exchange coupling in the case of half-occupied $d_{x^2-y^2}$ (a, top) and the interlayer exchange coupling in the case of half-occupied degenerate $d_{xz}d_{yz}$ (b, bottom). The upper line shows Fe d and/or O p orbitals, and the lower line shows their electronic configurations. The arrows show the spins of electrons. The broken arrows represent possible virtual hopping processes.

unpaired electrons of adjacent $d_{xz}d_{yz}$ orbitals, the electrons can be delocalized over the M−M unit, thus lowering the kinetic energy. If they are coupled ferromagnetically, the delocalized configurations are prevented by the exclusion principle. The intraplanar exchange interactions between $d_{xz}d_{yz}$ orbitals also show AFM coupling for the same reason. Therefore, the system shows a G type AFM order. Meanwhile, the orbitals exhibit ferro-orbital (FO) order; thus, the FO order supports the AF spin order, which is consistent with G-K rules.[20,21] Because the intraplanar σ bond is stronger than the interplanar π bond, the intraplanar exchange interaction is stronger than the interplanar exchange interaction.

The exchange parameters for this system can be estimated by using Heisenberg model[22] $H = -\sum_{i,j} J_{ij}\vec{S}_i\cdot\vec{S}_j$. Here we consider only the nearest neighbor (NN) intralayer Fe−O−Fe superexchange interaction J_1 and the NN interlayer Fe−Fe direct exchange interaction J_2 (Figure 1). The calculation gives $J_1 = -4.47$ meV and $J_2 = -1.78$ meV, and the ratio is $J_1/J_2 = 2.51$. This result is similar to that obtained in previous theoretical and experimental studies,[2−4] and it makes clear that it is the strong interlayer exchange interaction that supports the three-dimensional AFM state of the compound.

Next we checked the magnetic properties of the compound under pressure. We considered five kinds of magnetic order as

dx.doi.org/10.1021/ic401615r | Inorg. Chem. 2013, 52, 12529−12534

FM, AF1, AF2, AF3, AF4 and examined which kind of magnetic order would be the stable state at different pressures. The dependence of the site repulsion U on the pressure is still a controversial problem. Earlier research considered that U is independent of pressure,[23] while recent studies have pointed out that U is a function of pressure.[24]An increase of the screening effect between electrons with increasing pressure leads to a decrease of U, and a linear relation was suggested.[24,25] Therefore, it is reasonable not to consider U when higher pressure is applied. In fact, when we set U to the same value at ambient pressure (U = 5 eV), there is no pressure-induced spin transition, which is disagreement with experiment. If the U value is set according to the linear relation $U = 5 - P/10$, a spin transition from S = 2 to S = 1, accompanied by an AFM-FM transition, is observed at about 45 GPa (Figure 5), which is in

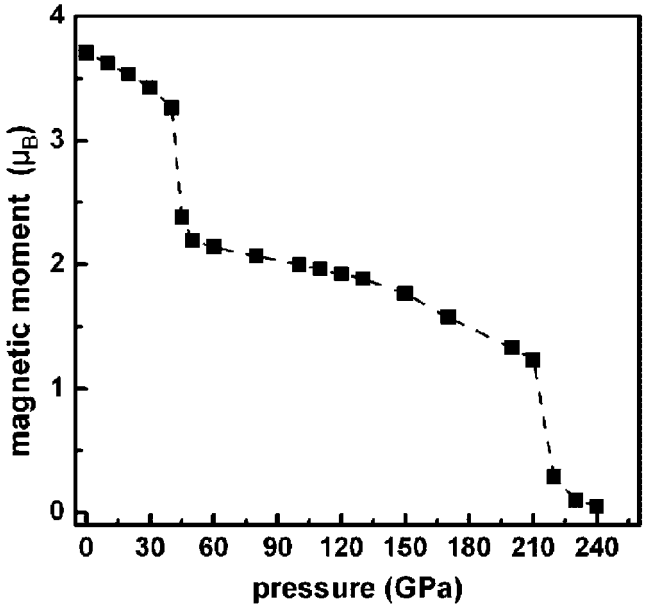

Figure 5. Pressure dependence of the magnetic moment of $SrFeO_2$.

reasonable agreement with experimental results.[8] It should be noted that the variation rate of U with the pressure greatly influences the calculated results. Rapid (or slow) decrease of U will lead to lower (or higher) transition pressure, or even no transition. Calculations using HSE06 also yield similar results when th eHartree−Fock mixing parameter in HSE06 decreases from 25% to 10%. Our results from DFT+U and HSE06 hybrid functional methods confirm the results of Kawakami et al. obtained on the basis of the PBE0 hybrid functional method and indicate a need to improve theoretical approaches.

To show how pressure affects the state, we approximately estimated the spin exchange splitting energy and the crystal field splitting energy of the Fe^{2+} d orbitals from their DOS. We find that the spin splitting energy becomes smaller with increasing pressure and the crystal field splitting energy for the d orbitals becomes larger, as indicated by Figure 2, while the densities of states for Fe 3d orbitals at different pressures are shown. With increasing pressure, intraplanar interaction between $d_{x^2-y^2}$ and p_σ causes the antibonding energy to increase, while the $d_{xz}d_{yz}$ antibonding energy decreases with decreasing displacement of adjacent Fe ions along the z axis. At a critical pressure, the major spin $d_{x^2-y^2}$ orbital becomes higher than the minor spin $d_{xz}d_{yz}$ orbital, the electron moves from the spin-up $d_{x^2-y^2}$ orbital to the spin-down $d_{xz}d_{yz}$ orbital, and then the $(d_{z^2})^2(d_{xz}d_{yz})^3(d_{xy})^1(d_{x^2-y^2})^0$ electronic configuration becomes stable; consequently, a spin transition from the high-spin (HS) state S = 2 to the intermediate-spin (IS) state S = 1 occurs. Although it is less common in comparison to the low-spin (LS) or HS state, the IS state of Fe^{2+} has been reported by Tarafder et al.[26] They explored a combination of DFT+U and ab initio molecular dynamic simulations to investigate the spin transition in the coordination polymer $Fe_2[Nb(CN)_8]\cdot(4\text{-pyridinealdoxime})_8\cdot 2H_2O$. They predicted the existence of an IS state of Fe^{2+} under pressure, and this IS state exhibited long-range FM coupling between the Fe and Nb spins, as opposed to long-range AF coupling between the HS Fe and Nb spins observed experimentally at ambient pressure. With increasing pressure, a spin transition from the IS state to LS state occurs. The Fe−Nb coordination polymer has distorted-octahedral FeN_6 coordination, while $SrFeO_2$ has square-planar FeO_4 coordination. The IS state of Fe^{2+} of $SrFeO_2$ under pressure is the first to be observed in square-planar coordination systems. This IS state exhibits FM coupling between Fe spins, while the HS state exhibits AF coupling, which is similar to the case for Fe−Nb systems. Tarafder et al. also studied the influence of substitution of Fe by Mn. In comparison with Fe−Nb, they noted that under pressure the Mn variant exhibits a one-step HS-LS transition. They attributed this to the larger HS moment of Mn in comparison to that of Fe and a stronger Mn−Nb magnetic interaction. It will be interesting to investigate the effect of substitution of Fe by Mn in $SrFeO_2$, which is our next work. Another example of an IS state of $3d^6$ configuration is Co^{3+} in $LaCoO_3$.[27] With an increase of temperature, $LaCoO_3$ undergoes a LS-IS-HS transition. The thermally induced spin transition of the Co^{3+} and pressure-induced spin transition of Fe^{2+} have the same features that the spin moment decreases with decreasing ion radius because of an increase of crystal-field splitting.

The pressure-induced electronic configuration transition of Fe 3d from $(d_{z^2})^2(d_{xz}d_{yz})^2(d_{xy})^1(d_{x^2-y^2})^1$ to $(d_{z^2})^2(d_{xz}d_{yz})^3(d_{xy})^1(d_{x^2-y^2})^0$ also leads to an AFM-FM transition. According to $(d_{z^2})^2(d_{xz}d_{yz})^3(d_{xy})^1(d_{x^2-y^2})^0$ occupation, the intralayer exchange interaction between two adjacent $d_{x^2-y^2}$ orbitals disappears, while two adjacent d_{xy} orbitals tend to retain the same AF couple as at ambient pressure. However, the intralayer exchange interactions between $d_{xz}d_{yz}$ orbitals of adjacent iron atoms differ from that at ambient pressure due to a different electronic configuration, as shown in Figure 6a. If two iron atoms couple ferromagnetically, the spin-down electron moves from an occupied orbital to an unoccupied orbital, thus lowering the kinetic energy. d_{yz} orbitals along the y direction also couple ferromagnetically for the same reason. However, along the z direction, the same mechanism causes the direct exchange interaction between $d_{xz}d_{yz}$ to be ferromagnetic (Figure 6b). In the x−y plane, there are two complete mechanisms, AF order and FM order, favored by d_{xy} and degenerate $d_{xz}d_{yz}$ orbitals, respectively. The latter mechanism is favored. Therefore, all intraplanar and interplanar exchanges show FM coupling.

When the pressure continues to increase, charge transfers from 2p orbitals of oxygen to 3d orbitals of Fe, and $d_{x^2-y^2}$ obtains electrons again, even though FM coupling is still stronger than AFM coupling. Although AFM exchange parameters increase with decreasing displacement of ions, a spin decrease due to a spin transition compensates for the effect of the increase of AFM exchange energy.[28,29] In contrast, FM

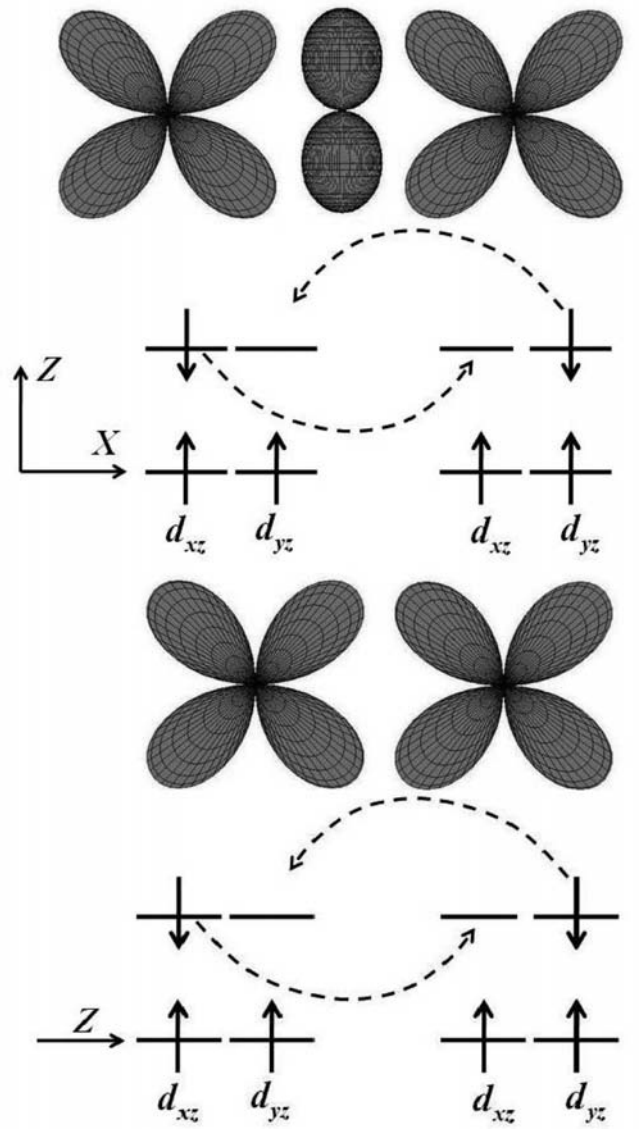

Figure 6. Illustrations of the intralayer exchange coupling (a, top) and interlayer exchange coupling (b, bottom) in the case of a singly occupied degenerate $d_{xz}d_{yz}$. For brevity, in the upper line only d_{xz} orbitals are depicted, while in the lower line the intermediate p_π orbitals which are active in the superexchange process are not shown. The arrows show the spins of electrons. The broken arrows represent possible virtual hopping processes.

coupling continues to increase with decreasing displacement of ions. As a consequence, the effect of FM coupling overcomes the effect of AFM coupling.

In addition to the spin state, other drastically changed parameters accompanying the magnetic state are the lattice constants, as indicated by Figure 7, where the dependence of the ratio c/a on the pressure is given. We can easily see that c/a experiences a jumping at ~45 GPa, and this is accompanied by a magnetic transition. The change of lattice constants can be explained by a change in the electronic configuration. When pressure is applied, both a and c decrease. However, a decreases more slowly than c because of the repulsive interaction between the electron in $d_{x^2-y^2}$ and negatively charged ligands in the ab plane; thus, c/a decreases with increasing pressure. When a spin transition occurs, the electron in $d_{x^2-y^2}$ moves to minority-spin $d_{xz}d_{yz}$ orbitals and a suffers a rapid decrease due to the

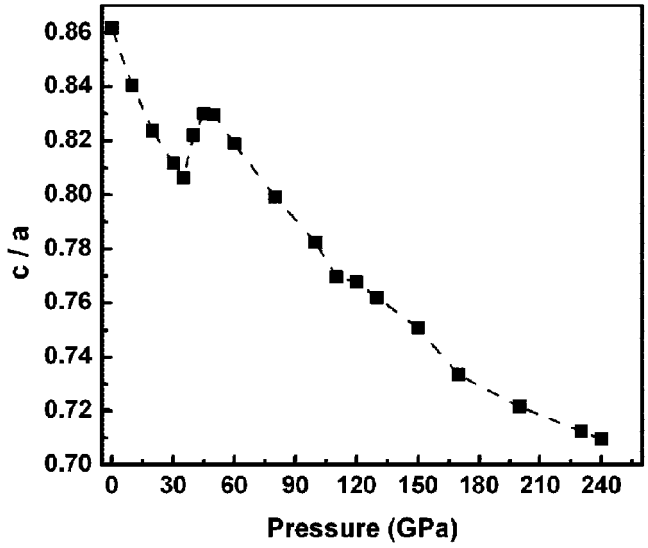

Figure 7. Pressure dependence of lattice parameter ratio c/a.

disappearance of this repulsive interaction and c/a increases suddenly. When pressure is applied further, electrons transfer from ligands to $d_{x^2-y^2}$ again, and this repulsive interaction makes a decrease more slowly than c again. Therefore, c/a decreases with increasing pressure again.

Finally, our calculations show than another spin transition from intermediate-spin state $S = 1$ to low-spin state $S = 0$ occurs at ~220 GPa (Figure 5). In contrast to the $S = 2$ to $S = 1$ spin transition, this transition is a second-order transition, because lattice parameters change continually as indicated by Figure 7.

IV. CONCLUSIONS

We have reported the results of the electronic structures and magnetism of $SrFeO_2$ under pressure. Several approaches have been used in our first-principles calculations, including GGA+U and HSE06. It is found that the site repulsion U and its pressure dependence are necessary to take into account in order to account for the antiferromagnetic state at ambient condition and the pressure-induced spin transition as well as the AFM–FM transition. The electronic configuration of the doubly occupied d_{z^2} orbital at ambient pressure, which inhibits Jahn–Teller distortion, can be qualitatively understood by an ionic model together with hybridization effects between the Fe 3d and O 2p states. In addition to the mechanism of spin transition, which was given by Kawakami et al.,[8] we find that the AF1 spin order at ambient pressure is due to the antiferromagnetic intraplane superexchange between the $d_{x^2-y^2}$ orbitals mediated by O p_σ orbitals and the antiferromagnetic interplane direct exchange between the $d_{xz}d_{yz}$ orbitals. The spin transition from the $S = 2$ to $S = 1$ state and the AFM-FM transition under pressure are reproduced, which are in reasonable agreement with experiment. It is found that the pressure induces a change in the electronic configuration of Fe 3d from $(d_{z^2})^2(d_{xz}d_{yz})^2(d_{xy})^1(d_{x^2-y^2})^1$ to $(d_{z^2})^2(d_{xz}d_{yz})^3(d_{xy})^1(d_{x^2-y^2})^0$; accordingly, the spin state changes from $S = 2$ to $S = 1$. Furthermore, the variation of the electronic configuration leads to a change in both intralayer superexchange coupling and interlayer direction exchange coupling between the Fe^{2+} ions from antiferromagnetic to ferromagnetic according to the G-K rules; as a result, a pressure-induced

dx.doi.org/10.1021/ic401615r | Inorg. Chem. 2013, 52, 12529–12534

AFM-FM transition occurs. Calculations also indicate that another spin transition from $S = 1$ to $S = 0$ may occur at about 220 GPa.

AUTHOR INFORMATION

Corresponding Author

*E-mail for G.-h.G.: guogh@mail.csu.edu.cn.

Notes

The authors declare no competing financial interest.

ACKNOWLEDGMENTS

This work was supported by the National Natural Science Foundation of China (No. 11374373), the Doctoral Fund of the Ministry of Education of China (No. 20120162110020), and the Natural Science Foundation of Hunan Province of China (No. 13JJ2004). M.R. acknowledges the support of the Fundamental Research Funds for CSU (No. 2012zzts005).

REFERENCES

(1) Tsujimoto, Y.; Tassel, C.; Hayashi, N.; Watanabe, T.; Kageyama, H.; Yoshimura, K.; Takano, M.; Ceretti, M.; Ritter, C.; Paulus, W. *Nature* **2007**, *450*, 1062−U8.

(2) Xiang, H. J.; Wei, S.-H.; Whangbo, M.-H. *Phys. Rev. Lett.* **2008**, *100*, 167207.

(3) Pruneda, J. M.; Iniguez, J.; Canadell, E.; Kageyama, H.; Takano, M. *Phys. Rev. B* **2008**, *78*, 115101.

(4) Tomiyasu, K.; Kageyama, H.; Lee, C.; Whangbo, M. H.; Tsujimoto, Y.; Yoshimura, K.; Taylor, J. W.; Llobet, A.; Trouw, F.; Kakuraim, K.; Yamada, K. *J. Phys. Soc. Jpn.* **2010**, *79*, 034707.

(5) Burns, R. G.; Clark, M. G.; Stone, A. J. *Inorg. Chem.* **1966**, *5*, 1268−1272.

(6) Tassel, C.; Pruneda, J. M.; Hayashi, N.; Watanabe, T.; Kitada, A.; Tsujimoto, Y.; Kageyama, H.; Yoshimura, K.; Takano, M.; Nishi, M.; Ohoyama, K.; Mizumaki, M.; Kawamura, N.; Iniguez, J.; Canadell, E. *J. Am. Chem. Soc.* **2009**, *131*, 221−229.

(7) Wells, A. F. *Structural Inorganic Chemistry*, 4th ed.; Oxford University Press: Oxford, U.K., 1975.

(8) Kawakami, T.; Tsujimoto, Y.; Kageyama, H.; Chen, X.-Q.; Fu, C. L.; Tassel, C.; Kitada, A.; Suto, S.; Hirama, K.; Sekiya, Y.; Makino, Y.; Okada, T.; Yagi, T.; Hayashi, N.; Yoshimura, K.; Nasu, S.; Podloucky, R.; Takano, M. *Nat. Chem.* **2009**, *1*, 371−376.

(9) Whangbo, M.-H.; Koehler, J. *Nat. Chem.* **2009**, *1*, 351−352.

(10) Kageyama, H.; Watanabe, T.; Tsujimoto, Y.; Kitada, A.; Sumida, Y.; Kanamori, K.; Yoshimura, K.; Hayashi, N.; Muranaka, S.; Takano, M.; Ceretti, M.; Paulus, W.; Ritter, C.; André, G. *Angew. Chem., Int. Ed.* **2008**, *47*, 5740−5745.

(11) Yamamoto, T.; Kobayashi, Y.; Hayashi, N.; Tassel, C.; Saito, T.; Yamanaka, S.; Takano, M.; Ohoyama, K.; Shimakawa, Y.; Yoshimura, K.; Kageyama, H. *J. Am. Chem. Soc.* **2012**, *134*, 11444−11454.

(12) Giannozzi, P.; Baroni, S.; Bonini, N.; Calandra, M.; Car, R.; Cavazzoni, C.; Ceresoli, D.; Chiarotti, G. L.; Cococcioni, M.; Dabo, I.; Corso, A. D.; Gironcoli, S. de; Fabris, S.; Fratesi, G.; Gebauer, R.; Gerstmann, U.; Gougoussis, C.; Kokalj, A.; Lazzeri, M.; Martin-Samos, L.; Marzari, N.; Mauri, F.; Mazzarello, R.; Paolini, S.; Pasquarello, A.; Paulatto, L.; Sbraccia, C.; Scandolo, S.; Sclauzero, G.; Seitsonen, A. P.; Smogunov, A.; Umari, P.; Wentzcovitch, R. M. *J. Phys.: Condens. Matter* **2009**, *21*, 395502.

(13) Perdew, J. P.; Burke, K.; Ernzerhof, M. *Phys. Rev. Lett.* **1996**, *77*, 3865−3868.

(14) Solovyev, I. V. *J. Phys.: Condens. Matter* **2008**, *20*, 293201.

(15) Anisimov, V. I.; Zaanen, J.; Andersen, O. K. *Phys. Rev. B* **1991**, *44*, 943−954.

(16) Vanderbilt, D. *Phys. Rev. B* **1990**, *41*, 7892−7895.

(17) Heyd, J.; Scuseria, G. E.; Ernzerhof, M. *J. Chem. Phys.* **2003**, *118*, 8207−8215.

(18) Hamann, D. R.; Schlüter, M.; Chiang, C. *Phys. Rev. Lett.* **1979**, *43*, 1494−1497.

(19) Fenske, R. F.; Martin, D. S.; Ruedenberg, K. *Inorg. Chem.* **1962**, *1*, 441−452.

(20) Goodenough, J. B.; Wold, A.; Arnott, R. J.; Menyuk, N. *Phys. Rev.* **1961**, *124*, 373−384.

(21) Kawakami, T.; Kageyama, H. *Z. Kristallogr.* **2010**, *225*, 504−507.

(22) Xiang, H.; Lee, C.; Koo, H.-J.; Gong, X.; Whangbo, M.-H. *Dalton Trans.* **2012**, *42*, 823−853.

(23) Massey, M. J.; Chen, N. H.; Allen, J. W.; Merlin, R. *Phys. Rev. B* **1990**, *42*, 8776−8779.

(24) Gavriliuk, A. G.; Trojan, I. A.; Struzhkin, V. V. *Phys. Rev. Lett.* **2012**, *109*, 086402.

(25) Cohen, R. E.; Mazin, I. I.; Isaak, D. G. *Science* **1997**, *275*, 654−657.

(26) Tarafder, K.; Kanungo, S.; Oppeneer, P. M.; Saha-Dasgupta, T. *Phys. Rev. Lett.* **2012**, *109*, 077203.

(27) Korotin, M. A.; Ezhov, S.Yu.; Solovyev, I. V.; Anisimov, V. I. *Phys. Rev. B* **1996**, *54*, 5309−5316.

(28) Mostovoy, M. *Phys. Rev. Lett.* **2005**, *94*, 137205.

(29) Li, L.; Wang, W.; Liu, H.; Liu, X.; Song, Q.; Ren, S. *J. Phys. Chem. C* **2009**, *113*, 8460−8464.